Crossover in growth laws for phase-separating binary fluids: Molecular dynamics simulations

Shaista Ahmad,[1,2] Subir K. Das,[1,*] and Sanjay Puri[2]

[1]*Theoretical Sciences Unit, Jawaharlal Nehru Centre for Advanced Scientific Research, Jakkur Post Office, Bangalore 560064, India*

[2]*School of Physical Sciences, Jawaharlal Nehru University, New Delhi 110067, India*

(Received 7 February 2012; published 27 March 2012)

Pattern and dynamics during phase separation in a symmetrical binary ($A + B$) Lennard-Jones fluid are studied via molecular dynamics simulations after quenching homogeneously mixed critical (50:50) systems to temperatures below the critical one. The morphology of the domains, rich in A or B particles, is observed to be bicontinuous. The early-time growth of the average domain size is found to be consistent with the Lifshitz-Slyozov law for diffusive domain coarsening. After a characteristic time, dependent on the temperature, we find a clear crossover to an extended viscous hydrodynamic regime where the domains grow linearly with time. Pattern formation in the present system is compared with that in solid binary mixtures, as a function of temperature. Important results for the finite-size and temperature effects on the small-wave-vector behavior of the scattering function are also presented.

DOI: 10.1103/PhysRevE.85.031140 PACS number(s): 64.60.−i, 29.25.Bx, 41.75.Lx

I. INTRODUCTION

When quenched inside the miscibility gap, a homogeneous binary ($A + B$) mixture, prepared at a high temperature, phase separates into coexisting A-rich and B-rich phases. Starting from the mixed phase, the system's progress toward the new equilibrium state is a complex nonlinear process [1–5] and proceeds via formation and growth of domains rich in A or B particles. This domain coarsening is a scaling phenomenon, e.g., the two-point equal-time (t) correlation function $C(r,t)$ (r being the separation between two points) and its Fourier transform, the structure factor $S(k,t)$ (k being the magnitude of the wave vector), obey the scaling forms:

$$C(r,t) \equiv g(r/\ell(t)), \tag{1}$$

$$S(k,t) \equiv \ell(t)^d f(k\ell(t)). \tag{2}$$

In Eqs. (1) and (2), $\ell(t)$ is the average size of domains at time t and d is the system dimensionality. Typically $\ell(t)$ grows in a power-law fashion as

$$\ell(t) \sim t^{\alpha}, \tag{3}$$

where the exponent α depends on the transport mechanism dominant during the coarsening process. There has been much recent interest [6–18] in understanding the pattern and dynamics in bulk phase separating systems as well as in systems under confinement. Below we summarize some of the primary results in the context of the kinetics of bulk phase separation.

For *diffusive* transport, relating the growth of domains with the chemical potential ($\mu = \gamma/\ell$, γ being the interfacial tension) gradient, one has

$$\frac{d\ell(t)}{dt} \propto \frac{1}{\ell}\frac{\gamma}{\ell} = \frac{\gamma}{\ell^2}. \tag{4}$$

Solution of Eq. (4) provides $\alpha = 1/3$, which is referred to as the Lifshitz-Slyozov (LS) [19] growth law and is found to be the primary mechanism in the kinetics of phase separation in binary solid mixtures. On the other hand, in fluids and polymers, hydrodynamics plays a very important role. In that case, one expects much faster coarsening due to advective transport of material [20–22]. For a critical quench, giving rise to an interconnected domain structure, in spatial dimension $d = 3$, one balances the surface energy density (γ/ℓ) and the viscous stress [$6\pi\eta v_\ell/\ell$, v_ℓ being the interface velocity and η the shear viscosity], to obtain

$$v_\ell = \frac{d\ell(t)}{dt} = \frac{\gamma}{6\pi\eta}. \tag{5}$$

Solution of Eq. (5) predicts a linear growth with $\alpha = 1$, a picture that holds for low Reynolds numbers and is referred to as the *viscous hydrodynamic* growth. A crossover from the diffusive to this linear regime is expected to occur for $\ell(t) \gg \ell_{\rm vis} \sim (D\eta)^{1/2}$, D being the diffusion constant. On the other hand, for $\ell(t) \gg \ell_{\rm in}$ [the inertial length $= \eta^2/(\rho\gamma)$, ρ being the density], the surface energy is balanced by the kinetic energy density $\rho v_\ell{}^2$, so that

$$\frac{d\ell(t)}{dt} = \left(\frac{\gamma}{\rho\ell}\right)^{1/2}. \tag{6}$$

This yields $\alpha = 2/3$, which is known as the *inertial hydrodynamic* growth exponent. In this work, however, we do not aim to obtain this growth regime. For off-critical quenches, however, where one has a droplet-like morphology of the minority component, a single regime with $\alpha = 1/3$ is expected from Brownian droplet diffusion and collision mechanism [23,24]. In this paper, we present extensive results for the situation where one has a critical composition of A and B particles. Some preliminary results on this topic were reported in a recent communication [7]. In this case, as discussed above, we anticipate three different regimes of growth, with exponents 1/3, 1, and 2/3, respectively. Of course, at very early times (for both solid and fluid mixtures) the possibility of an exponent 1/4 due to interface diffusion [25], particularly at very low temperatures, cannot be ruled out.

While a crossover from the diffusive to the viscous hydrodynamic regime was observed in experiments [26–28] and model H simulations [29,30], both viscous and inertial

*das@jncasr.ac.in

regimes were observed in lattice-Boltzmann simulations [3]. In the latter case, one essentially solves the model H equations for the coarse-grained density order parameter (ϕ) and velocity ($\vec{v}$) fields. Using the incompressibility condition ($\vec{\nabla}\cdot\vec{v}=0$), these can be written as (note that $\perp$ stands for the transverse component [3])

$$\frac{\partial\phi}{\partial t}+\vec{v}\cdot\vec{\nabla}\phi=D\nabla^2\mu, \tag{7}$$

$$\rho\frac{\partial\vec{v}(\vec{r},t)}{\partial t}=\eta\nabla^2 v-[\phi\vec{\nabla}\mu+\rho(\vec{v}\cdot\vec{\nabla})\vec{v}]_\perp, \tag{8}$$

where ρ is the density of the fluid. This model is a combination of the Cahn-Hilliard and Navier-Stokes equations [1,3], the latter being introduced to model the velocity field. On the other hand, molecular dynamics (MD) simulations, where hydrodynamics is naturally included, have been relatively rare, due primarily to their demanding nature in terms of computer time. Early MD simulations [31–33] have been inconclusive—either due to a lack of data over a significant period of time or due to inappropriate analysis of the results. Moreover, these early MD results were obtained for low-density fluids, where a possible coupling between liquid-liquid and gas-liquid transitions could have added further complexity. While recent focus has turned toward systems with realistic interactions and boundary conditions [9,10,16–18], our understanding of phase separation dynamics in bulk fluids, thus, remains incomplete.

In this paper, we present results from large-scale MD simulations, in conjunction with a numerical renormalization procedure [9,34]. We address questions related to the similarity in morphologies during kinetics of phase separation in fluids to that in solids. In addition, we make quantitative statements about the domain growth law. These state-of-the-art MD results provide the first unambiguous confirmation of a crossover from the LS to the viscous hydrodynamic regime. On the issue of pattern formation, our observation of a quantitative similarity between the domain morphologies in fluids and solids is significant and nullifies earlier claims [30] of dissimilar structures. These results comparing pattern formation in segregating solids and fluids have important theoretical implications, since a universal analytical form for the scaling function for phase-separating systems remains an outstanding task in this area. We quantify the structural details via calculations of $C(r,t)$ and $S(k,t)$. Our simulation results for $S(k,t)$, for deep quenches, obey

$$\begin{aligned} S(k,t)&\sim k^4, \quad k\to 0,\\ S(k,t)&\sim k^{-(d+n)}, \quad k\to\infty, \end{aligned} \tag{9}$$

where the former is known as Yeung's law [35] and the latter as the generalized Porod's law [36–38]. Note that in addition to the pattern dynamics in the density (concentration) field, we also explore the pattern formation in the velocity field. Thus, from here onward, the structure factors for the density and velocity fields are represented as $S_{\phi\phi}$ and S_{vv}, respectively. In Eq. (9), n is the order-parameter dimensionality, which has values $n=1$ for the density field and $n=3$ for the velocity field.

This paper is organized as follows. In Sec. II, we describe the details of the model and methodology. We present results for both structure and dynamics in Sec. III. Finally, in Sec. IV we conclude the paper with an outlook on future possibilities.

II. MODELS AND METHODS

For the study of phase separation in a binary fluid, we use a high-density ($\rho=1$) continuum model, where the ith and jth particles, at positions $\vec{r}_i$ and $\vec{r}_j$ ($r=|\vec{r}_i-\vec{r}_j|$), interact via the potential

$$u(\vec{r}_i,\vec{r}_j)=\begin{cases} U(r)-U(r_c)-(r-r_c)\left(\frac{dU}{dr}\right)_{r=r_c}, & r<r_c;\\ 0, & r>r_c. \end{cases} \tag{10}$$

In Eq. (10),

$$U(r)=4\varepsilon_{\alpha\beta}\left[\left(\frac{\sigma_{\alpha\beta}}{r}\right)^{12}-\left(\frac{\sigma_{\alpha\beta}}{r}\right)^{6}\right] \tag{11}$$

is the standard Lennard-Jones (LJ) pair potential. In Eq. (11), $\sigma_{\alpha\beta}$ is the interaction diameter between α and β [$\in(A,B)$] particles and $\varepsilon_{\alpha\beta}$ is the interaction strength. The cutoff distance r_c in Eq. (10) is introduced to facilitate faster computation. The presence of the third term on the right-hand side of Eq. (10), after a shifting of the potential by its value at $r=r_c$ (second term), ensures that both the potential and the forces are continuous for all values of r. For the choices

$$\begin{aligned} \varepsilon_{AA}&=\varepsilon_{BB}=2\varepsilon_{AB}=\varepsilon,\\ \sigma_{AA}&=\sigma_{BB}=\sigma_{AB}=\sigma,\\ m_A&=m_B=m \end{aligned} \tag{12}$$

(m being the mass), we have a fully symmetric model, which belongs to the Ising universality class of equilibrium critical phenomena. Its phase diagram is symmetric about the critical composition of 50% A and 50% B. We set $r_c=2.5\sigma$, according to convention. The phase behavior and equilibrium static as well as the dynamic critical properties of this model, with $k_BT_c\simeq 1.423\varepsilon$, are well studied [39–41]. For the sake of convenience, we set ε, k_B, m, and σ to unity. At the chosen density, $\rho=1$, the model is found to be nearly incompressible so that a coupling between a gas-liquid and a liquid-liquid transition is safely avoided. Also, for the temperature range of interest, we do not face any crystallization problems.

The phase-separation kinetics of the 50:50 LJ model was studied via MD simulations by quenching the homogeneous configurations, prepared at a very high temperature ($T=10$; far above T_c), below the critical temperature. The MD runs were performed by using the Verlet velocity algorithm [42,43] with periodic boundary conditions in all directions. The integration time step was set to $\Delta t=0.01\tau$, with the LJ time unit $\tau=(m\sigma^2/\varepsilon)^{1/2}=1$. This provides integration error within an acceptable limit. The temperature was controlled by the application of a Nosé-Hoover thermostat (NHT) [42], which is known to preserve hydrodynamics well. Of course, more advanced thermostats [44,45] have recently become available with better hydrodynamics-preserving capability. However, the NHT is adequate for our simulation. To ensure the usefulness of our methodology, the results obtained via the NHT are compared with those obtained by application

of an Andersen thermostat (AT) [42], which is stochastic in nature. Notice that the AT does not preserve hydrodynamics. Therefore, we expect the LJ-AT model to mimic the diffusive segregation, as in the binary solid mixtures.

For analysis of the results, the continuum fluid configurations were mapped onto a simple cubic lattice. A lattice site occupied by an A particle was assigned the spin value of $+1$, and that occupied by a B particle was assigned the value of -1. This ensures that the rest of the analysis is similar to the solid binary mixture, where the kinetics of phase separation was studied via Monte Carlo (MC) [46] simulations of the spin-1/2 Ising model,

$$H = -J \sum_{\langle ij \rangle} S_i S_j, \quad J = 1. \tag{13}$$

The critical temperature for this model in $d = 3$ is $T_c \simeq 4.51$. The conserved order-parameter dynamics, where the composition of A and B particles remains fixed, was implemented via the standard Kawasaki-exchange mechanism [47]. For an MC move, an interchange of positions between a pair of nearest-neighbor particles is attempted and accepted according to the standard Metropolis criterion [46]. This mimics the diffusive transport in solid mixtures. A single MC step consists of L^d trial moves, where L is the linear dimension of the cubic box used for the simulation. Again, we applied periodic boundary conditions in all directions. All results (for both solid and fluid mixtures) were presented after averaging over at least five independent initial configurations.

The correlation function was calculated as

$$C(r,t) = \langle S_i(t) S_j(t) \rangle. \tag{14}$$

For a conserved order-parameter system, $C(r,t)$ exhibits damped oscillations around 0, the value which it asymptotically decays to. The average domain size, $\ell(t)$, was obtained from the first zero crossing of $C(r,t)$. Of course, there exist other suitable definitions for computing $\ell(t)$, e.g., the inverse of the first moment of $S(k,t)$ and moments of the domain size distribution. We confirmed that all these definitions differ only by constant multiplicative factors. For the sake of brevity, we present results only from the first definition, mentioned above.

At high temperatures, bulk domains contain fluctuating spin clusters, with linear dimension of the equilibrium correlation length ξ. The presence of these impurity spins hampers the calculation of $\ell(t)$ significantly. Thus, we have calculated all the observables from the renormalized domain morphologies obtained after eliminating the thermal noise via a majority spin rule. In this method, a spin at a lattice site j is replaced by the sign of the majority of the spins sitting at j and its nearest neighbor [9]. Of course, depending on the proximity to the critical point, one may need to consider further neighbors as well. This numerical procedure [34] eliminates the thermal fluctuations in bulk domains.

III. RESULTS

In this section, we present results for both structure and dynamics. Unless otherwise mentioned, all results for the LJ fluid correspond to the case with the NHT.

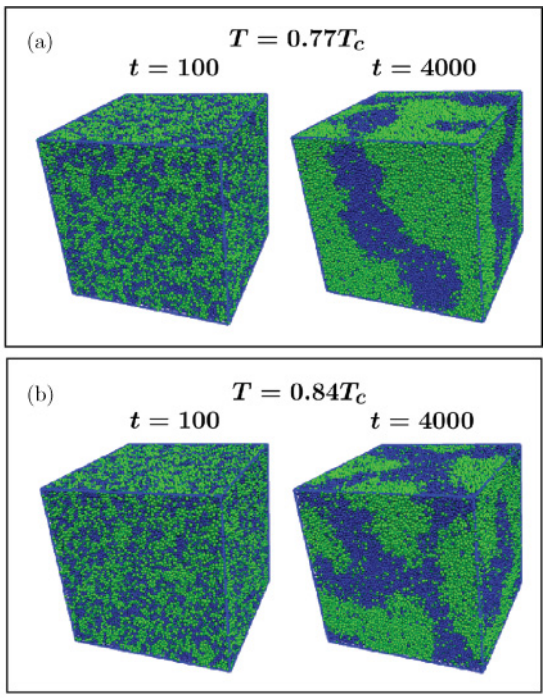

FIG. 1. (Color online) Three-dimensional snapshots during the molecular dynamics evolution of the symmetrical binary Lennard-Jones (LJ) fluid, starting from a homogeneously mixed system prepared at a high temperature ($\gg T_c$). Results for (a) $T = 1.1$ ($0.77T_c$) and (b) $T = 1.2$ ($0.84T_c$). For both temperatures we used systems of linear dimension $L = 64$. The times t mentioned are in LJ units. A particles are shown in black (blue) and B particles in gray (green).

A. Characterization of morphologies

Figure 1 shows the evolutionary snapshots of the binary LJ fluid obtained from our MD simulations at two different temperatures. Growth at the lower temperature appears to be faster than that at the higher temperature. This is because the surface tension γ, which provides the driving force for segregation, is higher for larger values of $(T_c - T)$. There is also a faster crossover, as demonstrated later, to the hydrodynamic regime at lower T. For a box of linear size $L = 64$, containing 262 144 particles, the system segregates completely after approximately $t = 8000$, at $T = 1.1$ ($=0.77T_c$). All results presented in the paper are from times significantly earlier than this time, so the data do not suffer from undesirable finite-size effects.

Another important difference between the snapshots at the two temperatures is in the noise level. As discussed earlier, at the higher temperature, the presence of spin clusters of length ξ [$\sim (T_c - T)^{-\nu}$; $\nu \simeq 0.63$] makes the unambiguous calculation of $\ell(t)$ very difficult. For this reason, we have eliminated the noise, employing the method discussed in the previous section. In Fig. 2(a), we compare an original configuration obtained at $t = 2000$ for $T = 1.2$ ($=0.84T_c$), with the corresponding renormalized snapshot (mapped to a simple cubic lattice). It is seen that our method preserves the domain morphology very well. For further check, 2-d cross-sectional views are shown in Fig. 2(b).

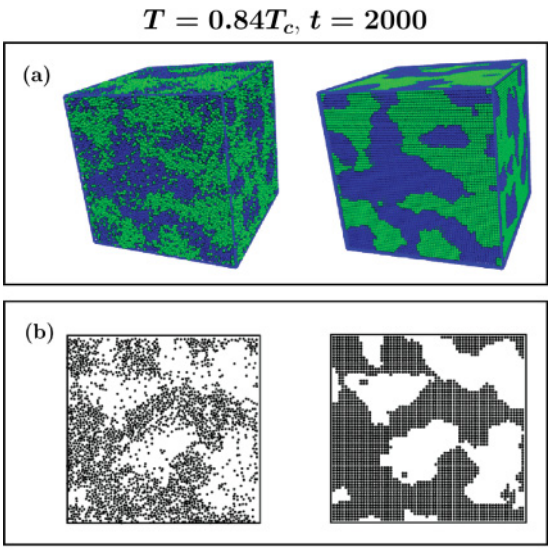

FIG. 2. (Color online) (a) Left: Three-dimensional snapshot at $t = 2000$ during the evolution of a binary LJ system with $L = 64$ at $T = 0.84T_c$. Right: The corresponding configuration after mapping onto a simple cubic lattice. Note that the noise seen in the original snapshot was removed in the mapped version by a majority particle renormalization procedure (see text for details). The same color coding is used as in Fig. 1. (b) Two-dimensional cuts of the configurations shown in (a). Again, the left one corresponds to the original continuum picture and the right one to the lattice configuration after removing the noise. Only A particles are shown.

In Fig. 3(a), we show a scaling plot of the correlation function for the LJ fluid at $T = 0.77T_c$. We plot $C(r,t)$ as a function of the scaled distance $r/\ell(t)$ at three times. The reasonably good data collapse suggests that a scaling regime has been reached. A similar exercise is done in Fig. 3(b) for another temperature, $T = 1.35$ (=$0.95T_c$). A difference that one observes between the two temperatures is in the amplitude of oscillation. In Fig. 3(c), we directly compare the scaling functions and, also, present results for one additional temperature, *viz.*, $T = 0.95$ (=$0.66T_c$). Essentially, at the temperature closest to T_c, the amplitude appears lower. Here we must mention that the scaling functions in domain growth are expected to be temperature independent. Indeed the correlation functions from $T = 0.66T_c$ and $0.77T_c$ are consistent with this fact. However, the deviation of the $T = 0.95T_c$ data set could well be due to interface roughening at T close to T_c and we expect it to overlap with the other two only at much later times. Note that there are corrections to scaling due to the factor ω/ℓ, where ω is the typical interface thickness. These become negligible when $\omega/\ell \to 0$, which occurs at delayed times, for larger values of ω.

Before discussing the above fact in greater detail, we ask whether there are morphological similarities of the fluid system to the solid mixture. The various lines in Fig. 3(c) denote the scaled correlation functions, obtained from the 3-d Ising model, at the corresponding temperatures ($0.66T_c$, $0.77T_c$, and $0.95T_c$). While the excellent agreement of data from fluid and solid confirms similar pattern formation, the strikingly similar temperature dependence of the scaling function in both cases is interesting.

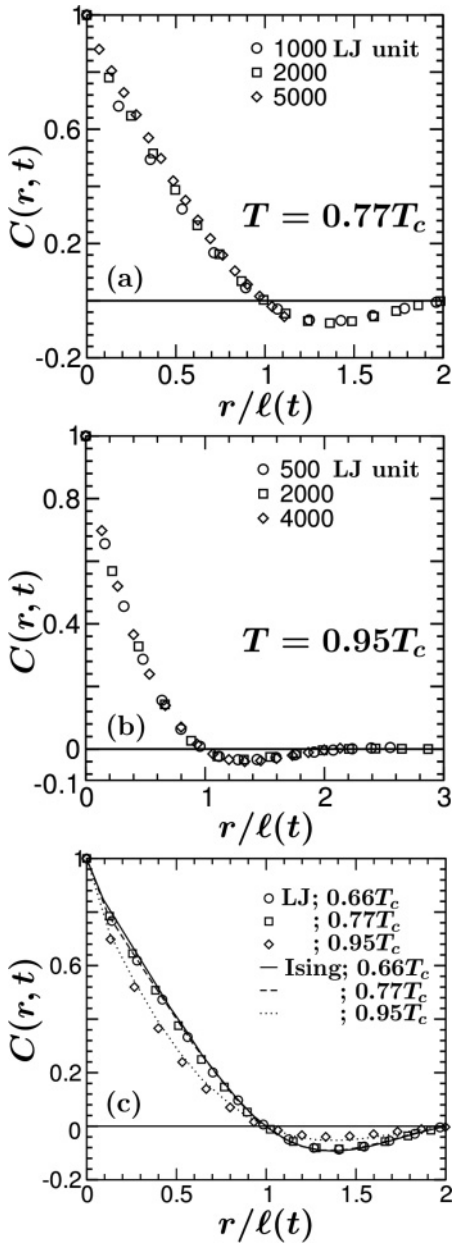

FIG. 3. (a) Scaling plot of $C(r,t)$ vs $r/\ell(t)$ at $T = 0.77T_c$ showing a collapse of the data, from three different times (as indicated), onto a single master curve. All results correspond to the LJ fluid. (b) Same as (a) but for $T = 0.95T_c$. (c) Comparison of the scaled correlation functions of the LJ fluid for three temperatures; solid, dashed, and dotted lines are corresponding functions obtained from the MC simulation of the Ising model at $0.66T_c$, $0.77T_c$, and $0.95T_c$, respectively.

To understand the reason behind this T dependence, we examine the evolution snapshots in Fig. 4. In Fig. 4(a), we show a 2-d cross section of the snapshots at $T = 0.77T_c$ and $0.95T_c$ for the LJ fluid. On the other hand, Fig. 4(b) shows the corresponding snapshots for the Ising solid. All the snapshots were obtained for the same system size and approximately the same domain size. The morphologies for the two systems at comparable temperatures are strikingly similar. The interfaces exhibit a more fractal structure at higher T values and are

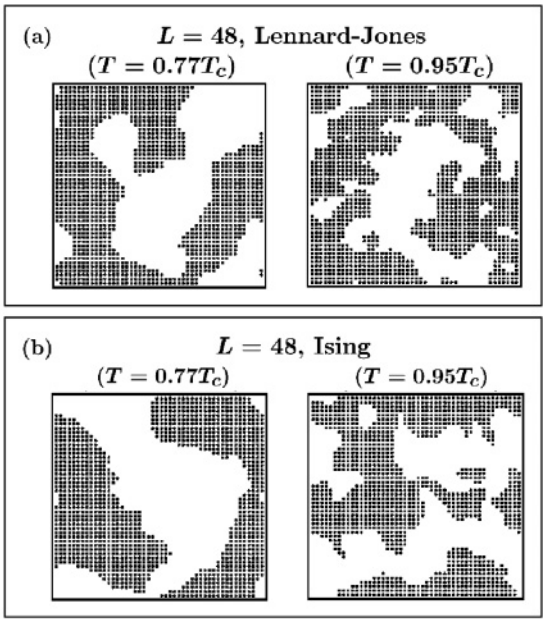

FIG. 4. (a) Two-dimensional cross sections of evolution snapshots for an LJ fluid at $T = 0.77T_c$ and $0.95T_c$ (as indicated), demonstrating the dissimilarities in pattern formation during phase separation for deep quench and quench close to criticality. For both temperatures, the snapshots correspond to an average domain size of $\simeq 12$ ($t = 2000$ LJ units for $0.77T_c$ and $t = 4000$ LJ units for $0.95T_c$). Note that only mapped and noise-eliminated pictures are shown. (b) Same as (a) but for the Ising model. Here the snapshot for $0.77T_c$ was obtained at $t = 25\,000$ MC steps and the one for $0.95T_c$ at $t = 13\,000$ MC steps. In both (a) and (b), only A particles are shown. Note that in (b) the second time is shorter than the first, as opposed to the situation in (a). This is due to the fact that in the case of solids there is no crossover to a faster-growing regime at lower temperatures (whereas in fluid, the crossover occurs more rapidly at lower temperatures, to the hydrodynamic regime).

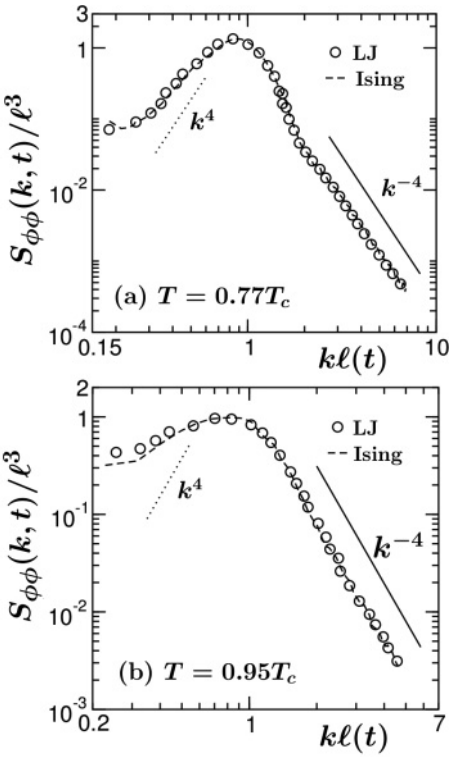

FIG. 5. (a) Scaling plot of the structure factor involving appropriate variables along the abscissa and ordinate. The circles correspond to the LJ fluid and the dashed line to the Ising solid, both being obtained at $T = 0.77T_c$. These master curves were obtained by combining results from different times. (b) Same as (a) but at $T = 0.95T_c$. The dotted line at the left corresponds to the expected increase in the structure factor according to the prediction of Yeung ($\propto k^4$), while the solid line at the right represents the Porod decay of the structure factor.

rougher at temperatures closer to T_c. Note that the interfaces are always rough for fluids with a higher roughness at larger T values. On the other hand, in 3-d Ising systems, one expects a roughening transition at $T = T_R \simeq 0.55T_c$ [48]. Below T_R, the interface is smooth, while for $T > T_R$, the width (ω) of the rough interface increases logarithmically with the system size. In a nonequilibrium situation like ours, the length analogous to the system size is the average domain size $\ell(t)$. Considering that $\ell(t)$ grows in a power-law fashion with time, one expects a logarithmic growth of ω with t. Since the growth of $\ell(t)$ is much faster than that, the contribution from the interface is expected to be negligible in the long-time limit (longer for higher temperatures) and the correlation function should have a universal shape independent of the temperature [49,50]. However, due to the limited access to time, we are unable to reach this asymptotic regime.

In Fig. 5, we compare the structure factors from the LJ and Ising systems at two temperatures. Again, for both temperatures there is a striking similarity between the Ising solid and the LJ fluid. These results are similar to the conclusion of Refs. [51] and [52], where the authors argued that the domain growth morphologies should be independent of kinetic mechanisms of coarsening. Those authors compared the structures arising from bulk diffusion of material with those from the interface diffusion. They found that the resultant structures are characterized by a universal scaling function. While our results show that this universality is of a more general validity, they are at variance with the findings of Ref. [30], which reported structural dissimilarity during the kinetics of phase separation in fluids and solids from simulations of *cell dynamical systems*. Reference [30] emphasizes the differences in the shoulder region of the scaled structure factors for segregating fluids and solids. However, the results presented here indicate that these differences are nonuniversal features arising from nonzero interfacial width.

The large-k structure factor data are in excellent agreement with the expected Porod law, $S(k,t) \sim k^{-(d+1)}$. While at the lower temperature, the small-k behavior of the structure factor is consistent with Yeung's prediction [$S(k,t) \sim k^4$], results at the higher temperature deviate from it. This could be understood as a consequence of the deviation of $C(r \gg 1)$ at the high temperature from the expected universal scaling behavior. Nevertheless, in Fig. 6 we take a closer look at the small-k behavior, where we present results only for the Ising model. This, as we will see, will provide further information related to finite-size effects.

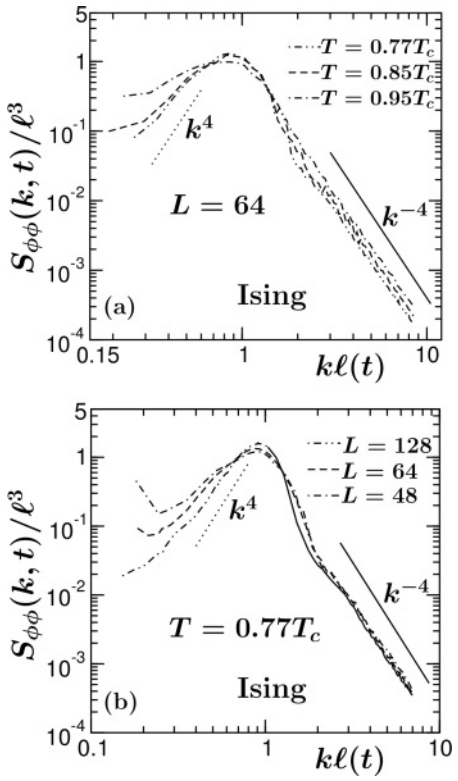

FIG. 6. (a) Plots of master curves for the Ising model structure factor at three temperatures, as indicated. All results were obtained for $L = 64$. The dotted straight line at the left corresponds to Yeung's law; the solid straight line at the right, to Porod's law. (b) Plots of master structure functions for three system sizes at $T = 0.77T_c$. Again, only the results for the Ising model are shown. In both (a) and (b), the objective is to demonstrate the small-wave-vector behavior.

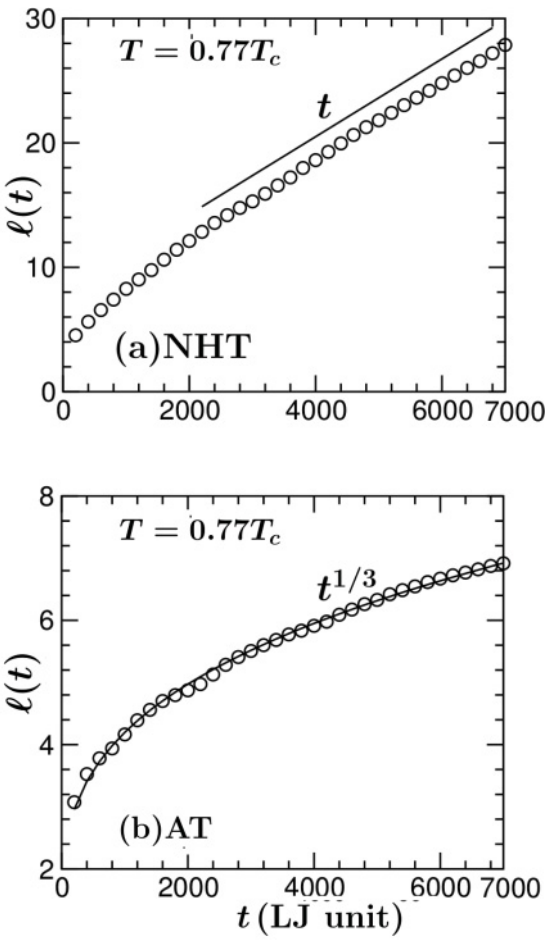

FIG. 7. (a) Plot of average domain size $\ell(t)$ as a function of time t for an LJ fluid, obtained from MD simulations using a Nosé-Hoover thermostat at $T = 0.77T_c$ with $L = 64$. The solid line corresponds to linear viscous hydrodynamic growth. (b) Plot of $\ell(t)$ vs t at the same temperature as in (a), but here, in MD simulations, the temperature was controlled through a stochastic Andersen thermostat. The solid line is a fit to the form Eq. (15).

Figure 6(a) shows the structure-factor scaling curves for a system of size $L = 64$ at three temperatures. It demonstrates gradual deviation from Yeung's law with increasing temperature. Of course, as pointed out in the context of $C(r,t)$, we need data at much longer times for temperatures very close to T_c to access the asymptotic regime. In addition, anticipating that finite-size effects could well be the reason behind this, we present in Fig. 6(b) the results for $T = 0.77T_c$ for three system sizes, as indicated. With an increase in system size, one sees a systematic trend toward a clearer k^4 increase for smaller k. Thus, here we conclude that, to confirm the temperature-independent universal behavior of the correlation function and structure factor, one needs to run big enough systems for much longer times.

B. Domain growth

Here, we present detailed results for the time dependence of the domain size. Figure 7(a) shows a plot of $\ell(t)$ vs t for an LJ fluid with a NHT, at $T = 0.77T_c$. The solid line denotes the linear viscous hydrodynamic growth regime. After a brief period of sublinear behavior, the data, starting from $t \simeq 2000$, are consistent with linear behavior. Note that we present data only up to $t = 7000$, because beyond this time we encountered finite-size effects. Before drawing a more concrete conclusion about this linear behavior, in Fig. 7(b) we examine a similar plot for the same system, but with the application of an AT. In this case, it is quite clear that the growth is much slower. This difference in results obtained via the NHT versus the AT is indeed expected, as discussed in the previous section. The solid line in Fig. 7(b) is a fit to the form

$$\ell(t) = B_1 + B_2 t^{1/3}. \tag{15}$$

A very good quality of fit confirms diffusive growth all along, as expected, due to the stochastic nature of the thermalization algorithm. On the other hand, no region in the data set in Fig. 7(a) provides even a reasonable fitting to the form Eq. (15). This confirms the utility of the NHT in the MD study of hydrodynamic phase separation.

The diffusive regime appears to be extremely short-lived at $T = 0.77T_c$. To obtain an appropriate confirmation of this expected early-time dynamics, in Fig. 8 we plot $\ell(t)$ vs t at a higher temperature, *viz.*, $0.95T_c$, where the crossover is delayed. Indeed, data for the whole time window show a good agreement with the $t^{1/3}$ behavior, shown by the solid line.

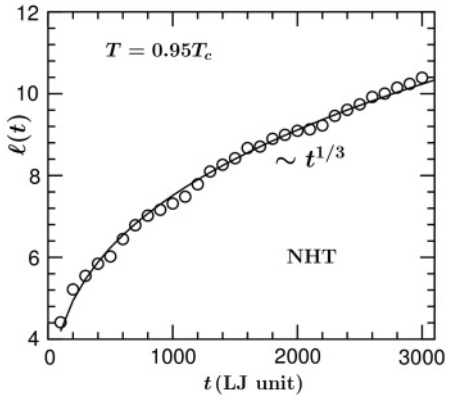

FIG. 8. Plot of $\ell(t)$ vs t for an LJ fluid at $T = 0.95T_c$ using an NHT. The solid line is a fit to the form Eq. (15).

Figure 9(a) shows a log-log plot of $\ell(t)$ vs t, for two temperatures, $T = 0.77T_c$ and $T = 0.88T_c$. From this figure it is quite clear that a crossover from a slower diffusive to a linear hydrodynamic behavior occurs very early at $T = 0.77T_c$. However, the data for $T = 0.88T_c$ show consistency with the $t^{1/3}$ behavior over a noticeable fraction of the time window,

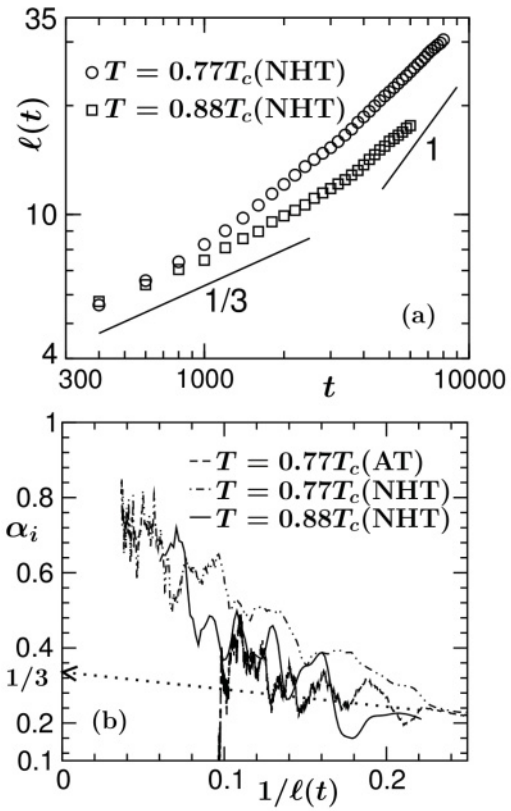

FIG. 9. (a) A log-log plot of $\ell(t)$ (obtained using the NHT) for an LJ fluid vs. t for two temperatures, as indicated. Solid lines correspond to diffusive (1/3) and viscous hydrodynamic (1) growth. (b) Plot of the instantaneous exponent α_i (see text for details) as a function of the inverse domain length, for both the AT and the NHT at $T = 0.77T_c$ and only for the NHT at $T = 0.88T_c$. The dotted arrow corresponds to a linear convergence to the value 1/3 in the case of pure diffusive growth.

before it gradually enters the viscous regime. In Fig. 9(b), we plot the instantaneous exponent α_i, calculated as

$$\alpha_i = \frac{d[\ln \ell(t)]}{d(\ln t)}, \tag{16}$$

as a function of $1/\ell(t)$. Here, two curves were obtained, at $T = 0.77T_c$ and $T = 0.88T_c$, by using the NHT, while the third curve (note that in this case a very long run length is required to match the x range of the other two curves) is for $T = 0.77T_c$ using the AT. As already mentioned, due to the stochastic nature of the AT, one expects that diffusive growth will be seen at all times [see Fig. 7(b)]. However, α_i smaller than 1/3, seen at early times, is due to the presence of a large offset at $t = 0$ [9]. The α_i is expected to converge to 1/3 (as shown by the dotted line) only in the limit $\ell(t) \to \infty$. The results for the NHT, on the other hand, look consistent with those for the AT at early times but deviate at later times, gradually converging to the exponent value 1.

To further confirm the hydrodynamic exponent, in the following we investigate the behavior of α_i in a different way. Here we introduce a time t_0 and assume that the growth kinetics follows a power-law behavior with time $t' = t - t_0$ as

$$\ell'(t') = \ell(t) - \ell(t_0) = B' t'^{\alpha} \tag{17}$$

and use this equation to calculate α_i $[=d(\ln \ell')/d(\ln t')]$. Equation (17) is invariant under an arbitrary choice of t_0 inside the linear regime. Thus, if t_0 is chosen appropriately (i.e., $t_0 > t_c$; the crossover time from a diffusive to a viscous hydrodynamic regime), $\alpha_i \simeq 1$ for all values of t'. However, as noted by other authors [9,30], in computer simulations with finite systems, one finds an oscillation of α_i around the expected value, the amplitude of which grows with the increase in ℓ. This is due to increasing separation between the domains of like particles, thus delaying effective collisions between them. Figure 10 plots α_i vs $1/\ell'$ for $t_0 = 2500$, which lies in the linear region [see Fig. 7(a)]. Indeed, this plot is consistent with the above expectation and α_i oscillates around the mean

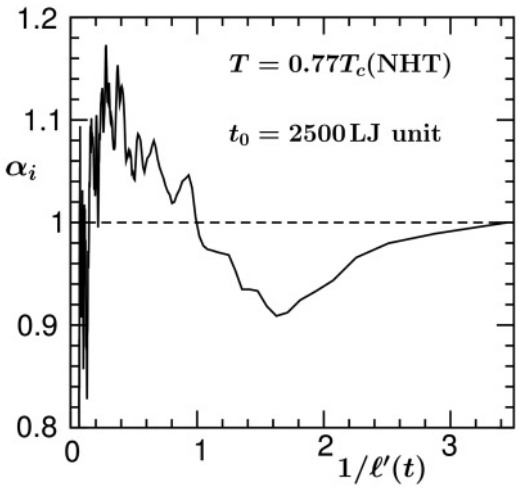

FIG. 10. Plot of α_i vs $1/\ell'(t)$ for $t_0 = 2500$ (see text for definitions of t_0 and ℓ'). The result is presented only for an LJ fluid with the NHT at $T = 0.77T_c$. The dashed horizontal line corresponds to viscous hydrodynamic growth.

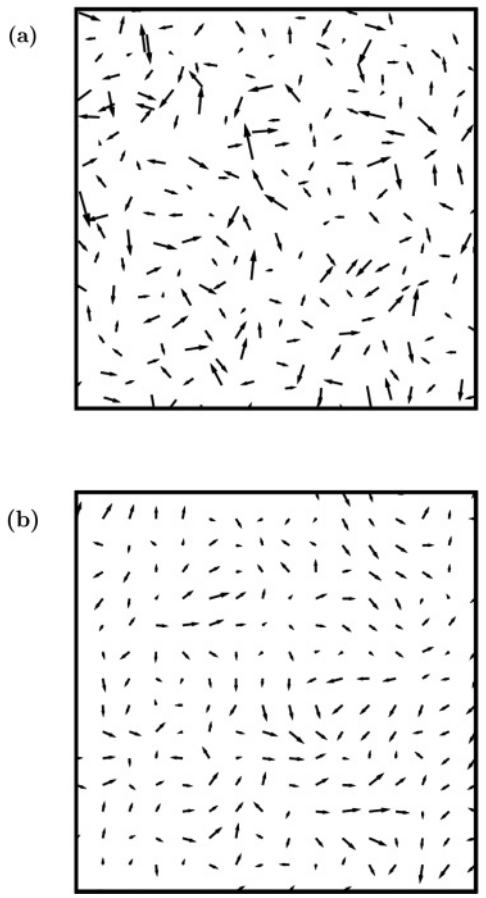

FIG. 11. (a) Part of a 2-d cross section showing the in-plane velocity field of the LJ particles with the NHT at $T = 0.77T_c$ with $L = 64$ at $t = 7000$. (b) A coarse-grained version of the snapshot shown in (a). Velocity vectors were coarse-grained by taking an average over all the particles contained in a $3\sigma \times 3\sigma \times 3\sigma$ cube symmetrically located around the point of interest.

value $\alpha_i \simeq 1$, providing an unambiguous confirmation of the viscous hydrodynamic growth law.

Finally, we present results for the velocity field. Figure 11(a) shows the 2-d cross section of the system evolved via the NHT at $T = 0.77T_c$ and $t = 7000$. The particle velocities are projected onto the plane. While in this picture, the orientations of the velocity vectors look quite random, interesting structure starts emerging upon coarse-graining over large length scales, as shown in Fig. 11(b). However, we have found the structure to be static in time and it is not characterized by a divergent length scale, unlike the findings of lattice-Boltzmann simulations [3,11]. It would be more interesting, though challenging, to study the dynamics of the velocity field in the neighborhood of the domain boundaries. Nevertheless, to characterize the structure shown in Fig. 11(b), which appears to be vortex-like (monopole in $d = 3$), in Fig. 12 we present the plot of structure factor $S_{vv}(k,t)$ vs k, on a log scale. The decay of the $S_{vv}(k,t)$ tail in fact follows the generalized Porod's law [38]. Note that for ordering of a three-component (for the velocity field, $n = 3$) vector order parameter field in $d = 3$, one expects $S_{vv} \sim k^{-6}$. This confirms the monopole-like defect formation (a point defect in $d = 3$), consistent with the pattern shown in Fig. 11(b).

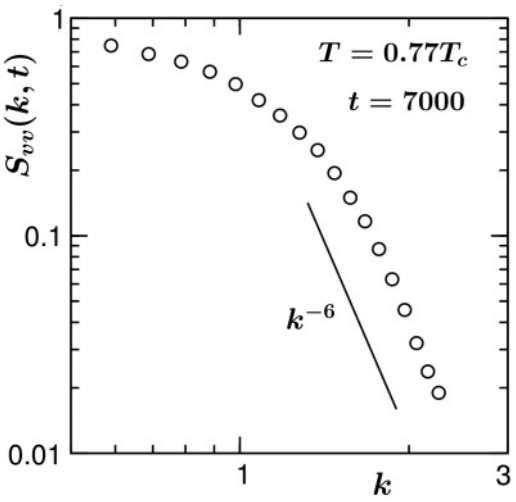

FIG. 12. Plot of $S_{vv}(k,t)$ vs k for a velocity field at $T = 0.77T_c$ and $t = 7000$ for an LJ fluid with the NHT. The solid line represents k^{-6} decay of the tail in accordance with the generalized Porod law.

IV. SUMMARY

We have presented results for the kinetics of phase separation in solid and fluid binary mixtures, the latter being the primary focus of the article. The results for fluid mixtures were obtained via MD simulations of a symmetric LJ model. On the other hand, for solid mixtures we have applied Kawasaki spin-exchange MC simulations to the Ising model.

Our extensive results confirm a striking similarity in pattern formation during phase separation in solid and fluid mixtures. This aspect has not been thoroughly explored previously. Even though the growth mechanisms in the two cases are different, this observation of similarities in domain morphologies is certainly interesting. We have also discussed the temperature and time dependence of structure in both cases. For the small-wave-vector behavior of the structure factor, we have provided comprehensive results for the corresponding finite-size effects as well.

Finally, this is the first MD work that unambiguously confirms the linear domain growth in the viscous hydrodynamic regime. We observe a clear crossover from a diffusive to a hydrodynamic regime. This is the first such observation, as far as MD results are concerned.

Even though our choice of system sizes appeared to be appropriate for obtaining viscous growth, they are not really big enough to study the growth in the inertial regime. To achieve the latter objective, multiscale modeling may be required, in addition to parallel programming and a graphics card [53].

In a future paper, we will address the aging properties of coarsening in this fluid model. Another interesting project would be to study domain growth with an off-critical composition, where hydrodynamic transport is effectively eliminated by lack of connectivity between domains.

ACKNOWLEDGMENTS

S.K.D. benefited from discussions with K. Binder and F. Corberi. Two of the authors (S.K.D. and S.A.) acknowledge financial support from the Department of Science and

Technology, India, via Grant No. SR/S2/RJN-13/2009. S.A. acknowledges the computational facility at the School of Physical Sciences, Jawaharlal Nehru University. S.A. is also grateful to the University Grants Commission, India, and the Jawaharlal Nehru Centre for Advanced Scientific Research for partial support.

[1] A. J. Bray, Adv. Phys. **51**, 481 (2002).
[2] K. Binder, in *Phase Transformation of Materials*, *Vol. 5*, edited by R. W. Cahn, P. Haasen, and E. J. Kramer (VCH, Weinheim, 1991), p. 405.
[3] S. Puri and V. Wadhawan (eds.), *Kinetics of Phase Transitions* (CRC Press, Boca Raton, FL, 2009).
[4] R. A. L. Jones, *Soft Condensed Matter* (Oxford University Press, Oxford, 2008).
[5] A. Onuki, *Phase Transition Dynamics* (Cambridge University Press, Cambridge, 2002).
[6] K. Nam, B. Kim, and S. J. Lee, J. Stat. Mech. Theory Exp. (2011) P03013.
[7] S. Ahmad, S. K. Das, and S. Puri, Phys. Rev. E **82**, 040107 (2010).
[8] S. Majumder and S. K. Das, Europhys. Lett. **95**, 46002 (2011).
[9] S. Majumder and S. K. Das, Phys. Rev. E **81**, 050102 (2010).
[10] S. J. Mitchell and D. P. Landau, Phys. Rev. Lett. **97**, 025701 (2006).
[11] V. M. Kendon, M. E. Cates, I. Pagonabarraga, J. C. Desplat, and P. Blandon, J. Fluid Mech. **440**, 147 (2001).
[12] H. Kabrede and R. Hentschke, Physica A **361**, 485 (2006).
[13] N. Blondiaux, S. Morgenthaler, R. Pugin, N. D. Spencer, and M. Liley, Appl. Surf. Sci. **254**, 6820 (2008).
[14] J. Liu, X. Wu, W. N. Lennard, and D. Landheer, Phys. Rev. B **80**, R041403 (2009).
[15] A. Sicilia, Y. Sarrazin, J. J. Arenzon, A. J. Bray, and L. F. Cugliandolo, Phys. Rev. E **80**, 031121 (2009).
[16] K. Bucior, L. Yelash, and K. Binder, Phys. Rev. E **77**, 051602 (2008).
[17] S. K. Das, S. Puri, J. Horbach, and K. Binder, Phys. Rev. Lett. **96**, 016107 (2006).
[18] M. J. A. Hore and M. Laradji, J. Chem. Phys. **132**, 024908 (2010).
[19] I. M. Lifshitz and V. V. Slyozov, J. Phys. Chem. Solids **19**, 35 (1961).
[20] E. D. Siggia, Phys. Rev. A **20**, 595 (1979).
[21] H. Furukawa, Phys. Rev. A **31**, 1103 (1985).
[22] H. Furukawa, Phys. Rev. A **36**, 2288 (1987).
[23] K. Binder and D. Stauffer, Phys. Rev. Lett. **33**, 1006 (1974).
[24] K. Binder, Phys. Rev. B **15**, 4425 (1977).
[25] S. Puri, A. J. Bray, and J. L. Lebowitz, Phys. Rev. E **56**, 758 (1997).
[26] Y. C. Chou and W. I. Goldburg, Phys. Rev. A **20**, 2105 (1979).
[27] N. C. Wong and C. M. Knobler, Phys. Rev. A **24**, 3205 (1981).
[28] F. S. Bates and P. Wiltzius, J. Chem. Phys. **91**, 3258 (1989).
[29] S. Puri and B. Dünweg, Phys. Rev. A **45**, R6977 (1992).
[30] A. Shinozaki and Y. Oono, Phys. Rev. E **48**, 2622 (1993).
[31] M. Laradji, S. Toxvaerd, and O. G. Mouritsen, Phys. Rev. Lett. **77**, 2253 (1996).
[32] A. K. Thakre, W. K. den Otter, and W. J. Briels, Phys. Rev. E **77**, 011503 (2008).
[33] W. J. Ma, A. Maritan, J. R. Banavar, and J. Koplik, Phys. Rev. A **45**, R5347 (1992).
[34] S. K. Das and S. Puri, Phys. Rev. E **65**, 026141 (2002).
[35] C. Yeung, Phys. Rev. Lett. **61**, 1135 (1988).
[36] G. Porod, *Small-Angle X-Ray Scattering*, edited by O. Glatter and O. Kratky (Academic Press, New York, 1982).
[37] Y. Oono and S. Puri, Mod. Phys. Lett. B **2**, 861 (1988).
[38] A. J. Bray and S. Puri, Phys. Rev. Lett. **67**, 2670 (1991).
[39] S. K. Das, M. E. Fisher, J. V. Sengers, J. Horbach, and K. Binder, Phys. Rev. Lett. **97**, 025702 (2006).
[40] S. K. Das, J. Horbach, K. Binder, M. E. Fisher, and J. V. Sengers, J. Chem. Phys. **125**, 024506 (2006).
[41] S. Roy and S. K. Das, Europhys. Lett. **94**, 36001 (2011).
[42] D. Frenkel and B. Smit, *Understanding Molecular Simulations: From Algorithms to Applications* (Academic Press, San Diego, California, 2002).
[43] M. P. Allen and D. J. Tildesly, *Computer Simulations of Liquids* (Clarendon, Oxford, 1987).
[44] S. D. Stoyanov and R. D. Groot, J. Chem. Phys. **122**, 114112 (2005).
[45] M. P. Allen and F. Schmid, Mol. Simul. **33**, 21 (2007).
[46] D. P. Landau and K. Binder, *A Guide to Monte Carlo Simulations in Statistical Physics* (Cambridge University Press, Cambridge, 2005).
[47] K. Kawasaki, *Phase Transition and Critical Phenomena,* Vol. 2, edited by C. Domb and M. S. Green (Academic Press, New York, 1972), p. 443.
[48] M. Hasenbusch and K. Pinn, J. Phys. A **30**, 63 (1997).
[49] S. Puri and Y. Oono, J. Phys. A **21**, L755 (1988).
[50] Y. Oono and S. Puri, Mod. Phys. Lett. B **2**, 861 (1988).
[51] S. Puri, A. J. Bray, and J. L. Lebowitz, Phys. Rev. E **56**, 758 (1997).
[52] S. van Gemmert, G. T. Barkema, and S. Puri, Phys. Rev. E **72**, 046131 (2005).
[53] B. J. Block, P. Virnau, and T. Preiss, Comput. Phys. Commun. **181**, 1549 (2010).